Modeling of the seat dip effect using the finite-difference time-domain method

Joe LoVetri[a)]

Department of Electrical Engineering, The University of Western Ontario, London, Ontario N6A 5B9, Canada

Doru Mardare[b)]

Department of Electrical Engineering, The University of Western Ontario, London, Ontario N6A 5B9, Canada

Gilbert Soulodre[c)]

Department of Psychology, Carleton University, 1125 Colonel By Drive, Ottawa, Ontario K1S 5B6, Canada

In this paper the use of the finite-difference time-domain technique for the modeling of the seat dip effect in concert halls is demonstrated. The linear time-domain acoustic partial differential equations are discretized using a finite-difference technique. The second-order accurate differencing scheme is time–space centered, and the velocity and pressure are solved on an interlaced mesh. First- and second-order Mur absorbing boundary conditions, originally formulated for electromagnetic problems, are adapted to the acoustics case and used to truncate the numerical grid. The technique is first verified by comparing the numerical results to the analytic solution of a simple point source. Results from computer simulations of the seat dip phenomena are compared with the findings of previous studies where measurements had been made on scale models and in real concert halls. The computer model successfully predicts the effects associated with the source–receiver distance, the height of the receiver, and the height of the source. © *1996 Acoustical Society of America.*

INTRODUCTION

The computer modeling of room acoustics has been traditionally limited to the image source method and ray tracing methods. These are high-frequency techniques which model the propagation of sound as rays, cones, or images, and generally do not include diffraction effects. That is, they do not directly model the wave nature of sound. More advanced ray tracing techniques do exist which approximate the diffraction phenomenon.[1,2] In order to investigate low-frequency phenomena, scale models are sometimes used. The main problem with these models is the expense and time required to obtain accurate results. Thus, it would be valuable to have a computer modeling technique which can efficiently model the correct physics of room acoustics based on the governing partial differential equations.

The partial differential equations governing acoustic phenomena can be cast in the frequency domain or the time domain. An important advantage of solving the time-domain equations is that the complete frequency response, in the band of frequencies contained in the excitation, can be obtained in one simulation. Furthermore, transient effects are easily observed in the time-domain approach. Therefore, in this paper we solve the time-domain partial differential equations which govern the propagation of acoustic waves.

Two general computational techniques for solving these partial differential equations are the finite-difference and finite-element methods. Both provide accurate solutions to the acoustic equations, but when dealing with room acoustics the main difficulty in applying either of these methods is the large amount of computer resources required to obtain useful results. This is mainly due to the size of the problems encountered in room acoustics. In general, finite-element techniques tend to be more computationally demanding due to the fact that irregular grids, with their associated large computational overhead, can be used to discretize the problem. Of course, the conforming of grids to object boundaries is a big advantage in terms of accuracy, but this advantage is not clear for time-domain problems. This is due to the fact that irregular grids tend to distort the propagation of acoustic energy and reduce the accuracy gained by better modeling of the object boundaries. The overhead required in finite-element programs generally makes them more demanding on memory and processing time than finite-difference techniques. Formulating finite-difference methods on irregular grids is, of course, possible, but it shares many of the same advantages and disadvantages over simple cubical grid finite-difference time-domain methods.

Finite-difference techniques which use uniform cubical grids are more computationally efficient than finite-element methods. They can be used to solve any of the various forms of time-domain equations which govern the acoustic field (i.e., second-order wave equation, first-order Newton and continuity equations, etc.).[3,4] In this paper we choose to solve the first-order equations using a second-order accurate differencing scheme which is time–space centered. This time–

[a)]Electronic mail: joe@gauss.engga.uwo.ca
[b)]Now with Institute for Computers 167, Calea Floreasca, 72321 Bucharest, Romania.
[c)]Electronic mail: gilbert@dgbt.doc.ca

space centering is in the spirit of the Yee algorithm used extensively in time-domain electromagnetic calculations.[5,6] A similar technique to the one presented in this work was recently derived independently of ours and presented in Ref. 7.

Even for finite-difference techniques the modeling of an entire concert hall would require more computer resources than are typically available on engineering workstations. On the other hand, many low-frequency phenomena which occur in concert halls can be modeled with modest computer resources. One such phenomena which we investigate in this study is the seat dip effect which occurs in concert halls.[10]

I. FINITE-DIFFERENCE TIME-DOMAIN SOLUTION OF ACOUSTIC EQUATIONS

A. The acoustic equations: Total and scattered field formulations

If we consider a gas having negligible viscosity, and assume that perturbations from rest conditions of the field variables, that is, velocity and pressure of the gas, are small, then the equations which govern the motion of the gas are Newton's equation[3]

$$\delta_0 \ \partial_t \boldsymbol{u} = -\boldsymbol{\nabla} p, \tag{1}$$

and the continuity equation

$$\partial_t p = -\delta_0 c^2 \boldsymbol{\nabla} \cdot \boldsymbol{u}, \tag{2}$$

where the notation ∂_t denotes partial differentiation with respect to time, δ_0 is the density of the gas at rest, p_0 is the pressure of the gas at rest, γ is the ratio of specific heat at constant pressure to that at constant volume ($\gamma = 1.4$ for air at normal temperature and pressure), $\boldsymbol{u}$ is the gas particle velocity, and p is the excess pressure (difference between actual pressure and p_0). The wave velocity is given by

$$c^2 = \gamma(p_0/\delta_0). \tag{3}$$

This final result can be easily seen, since by differentiating (2) with respect to t and using (1) we get the wave equation

$$\nabla^2 p - c^{-2} \ \partial_t^2 p = 0 \tag{4}$$

for the excess pressure. (A similar equation can be derived for the velocity $\boldsymbol{u}$.) Now many numerical techniques for acoustics start with this second-order wave equation. We choose to solve the first-order equations (1) and (2) directly.

We first write out the first-order equations in component form by using $\boldsymbol{u} = u_x \mathbf{a}_x + u_y \mathbf{a}_y + u_z \mathbf{a}_z$, where $\mathbf{a}_x$, $\mathbf{a}_y$, and $\mathbf{a}_z$ are the unit vectors in rectangular coordinates, and we make the substitution $q = -\delta_0^{-1} p$ which we call the normalized negative pressure to get

$$\partial_t u_x = \partial_x q, \tag{5}$$

$$\partial_t u_y = \partial_y q, \tag{6}$$

$$\partial_t u_z = \partial_z q, \tag{7}$$

$$\partial_t q = c^2 (\partial_x u_x + \partial_y u_y + \partial_z u_z). \tag{8}$$

The interesting aspect of these equations is that the time derivative of any velocity component is dependent only on spatial derivatives of the pressure. Similarly, the time derivative of the pressure is only related to spatial derivatives of the velocity. This special structure in the first-order equations will be taken advantage of to construct a numerical scheme wherein the velocity and pressure are interlaced in space and time.

In problems where a known incident field in a homogeneous region impinges on physical scatterers, it is more convenient to use the scattered field formulation.[3,4] In this formulation the total field is split up as the sum of the incident and scattered field. For example, $q = q^i + q^s$, where the i and s superscripts denote the incident and scattered field, respectively. In the homogeneous region surrounding the scatterers, the scattered field will satisfy the same equations as the total field, i.e., Eqs. (5)–(8). On the other hand, inside simple penetrable objects, which can be modeled by imposing a different speed of sound inside the object, or at the boundaries of perfectly hard or soft objects, the scattered field will be coupled to the incident field. For the case of simple penetrable objects, the coupling of the two fields occurs within the differential equations, whereas for the case of perfectly hard or soft objects the coupling occurs in the boundary conditions. Thus, for instance, inside a body made of a material in which the speed of sound within it is given as c_1, the continuity equation for the scattered field becomes

$$\partial_t q^S = c_1^2 (\partial_x u_x^S + \partial_y u_y^S + \partial_z u_z^S) + (c_1^2 - c^2)$$
$$\times (\partial_x u_x^i + \partial_y u_y^i + \partial_z u_z^i), \tag{9}$$

where now, since the incident field is given, the second term on the right-hand side acts as a source term for the scattered field. Newton's equations for the scattered field may be handled by a similar procedure when the density of the scatterer, δ_0, is different than the surrounding medium.

Acoustically hard objects are defined by imposing the condition that the velocity normal to the boundary goes to zero. On the other hand, the pressure at the boundaries of acoustically soft objects goes to zero. Mathematically we impose $\mathbf{n} \cdot \boldsymbol{u} = 0$, where $\mathbf{n}$ is the normal to the boundary of acoustically hard objects, and we impose $p = 0$ at the boundary of acoustically soft objects. Note that at the boundary of stationary hard objects we can equivalently write $\mathbf{n} \cdot \boldsymbol{\nabla} p = \partial_n p = 0$ from Newton's law. In the scattered field formulation these simply become $\mathbf{n} \cdot \boldsymbol{u}^s = -(\mathbf{n} \cdot \boldsymbol{u}^i)$, $p^s = -p^i$, and $\partial_n p^s = \partial_n p^i$, where on the boundary the incident field values $\boldsymbol{u}^i$, and p^i would be specified.

B. The finite-difference time-domain scheme

In what follows we approximate the first-order derivatives in equations (5)–(8) by the second-order centered difference form given by

$$\partial_\xi f(\xi)|_{\xi = \xi + \Delta \xi/2} = \frac{f(\xi + \Delta \xi) - f(\xi)}{\Delta \xi} + O(\Delta \xi^2), \tag{10}$$

and use the notation

$$f^n(i,j,k) = f(i\Delta x, \ j\Delta y, \ k\Delta z, \ n\Delta t) \tag{11}$$

for the grid function $f^n(i,j,k)$ defined on a grid with space–time cell size $\Delta x \times \Delta y \times \Delta z \times \Delta t$. We define the grid func-
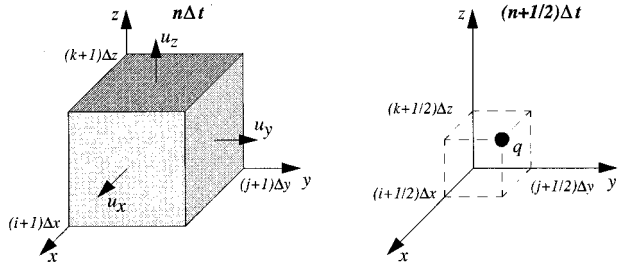
FIG. 1. Space-time interlacing of pressure and velocity in the numerical grid.

FIG. 2. Imposition of boundary conditions for acoustically hard and soft boundaries.

tion for negative pressure at the center of a cell and grid functions for the velocities normal to the faces of the cells. This configuration is depicted in Fig. 1. If the second-order finite-difference approximation given in Eq. (10) is used to approximate the time and space derivatives in Eqs. (5)–(8), then we can write

$$u_x^{n+1}(i) = u_x^n(i) + (\Delta t/\Delta h)[q^{n+1/2}(i+1/2)$$
$$- q^{n+1/2}(i-1/2)], \tag{12}$$

$$u_y^{n+1}(j) = u_y^n(j) + (\Delta t/\Delta h)[q^{n+1/2}(j+1/2)$$
$$- q^{n+1/2}(j-1/2)], \tag{13}$$

$$u_z^{n+1}(k) = u_z^n(k) + (\Delta t/\Delta h)[q^{n+1/2}(k+1/2)$$
$$- q^{n+1/2}(k-1/2)], \tag{14}$$

$$q^{n+1/2} = q^{n-1/2} + (\Delta t/\Delta h)c^2(u_x^n(i+1) - u_x^n(i)$$
$$+ u_y^n(j+1) - u_y^n(j) + u_z^n(k+1) - u_z^n(k)), \tag{15}$$

where all missing spatial indices are 1/2 indices. For example,

$$q^{n+1/2}(i+1/2) \Rightarrow q^{n+1/2}(i+1/2, j+1/2, k+1/2), \tag{16}$$

$$u_z^{n+1}(k) \Rightarrow u_z^{n+1}(i+1/2, j+1/2, k) \tag{17}$$

and we have chosen a cubical grid such that $\Delta x = \Delta y = \Delta z = \Delta h$.

The above interlaced leapfrog scheme is conditionally stable with Courant number $1/\sqrt{3}$, which means that the stability condition

$$c\Delta t/\Delta h \leq 1/\sqrt{3} \tag{18}$$

must be satisfied. The numerical dispersion of this scheme has been investigated previously.[6,7]

With the above scheme it becomes a simple matter to model acoustically hard boundaries where the velocity normal to the boundary goes to zero and acoustically soft boundaries where the pressure at the boundary goes to zero. We align soft boundaries with cell centers and set the pressure there to be zero. We align hard boundaries with cell faces and either set the normal velocity at that cell face to zero or we use the condition that the normal derivative of the pressure be zero. Referring to Fig. 2, the soft boundary is modeled by setting
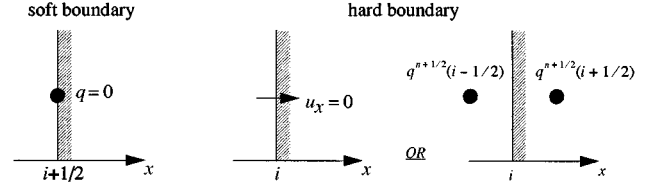
$$q^{n+1/2}(i+1/2) = 0, \tag{19}$$

and the hard boundary is modeled by setting

$$u_x^n(i) = 0 \quad \text{or} \quad q^{n+1/2}(i+1/2) = q^{n+1/2}(i-1/2) \tag{20}$$

for all time steps n.

Although we do not consider herein specific numerical examples of simple inhomogeneous materials, wherein the sound velocity is a function of position, these materials can be modeled simply by spatially discretizing the velocity parameter c as $c(i+1/2, j+1/2, k+1/2)$, and the density as $\delta_0 = \delta_0(i+1/2, j+1/2, k+1/2)$. Slightly more complicated formulations would be required for modeling materials exhibiting absorption (i.e., lossy materials), but the finite-difference method could be applied in a similar manner to those formulations.

C. Absorbing boundary conditions

Since the basic leapfrog scheme is space centered, numerical boundary conditions are required at the boundaries of the grid. The purpose of these numerical boundary conditions is to absorb the acoustic energy impinging on the boundaries from all angles, and therefore these conditions are sometimes called absorbing boundary conditions (ABCs). Much research has been performed on absorbing boundary conditions for wave-type equations.[6–9] Some of the characteristics used in judging the performance of ABCs are: (1) their ability to absorb energy at all angles of incidence; and (2) their ability to absorb at low as well as high frequencies.

Normally acoustic energy scattered from arbitrary obstacles will impinge on the outer boundary at arbitrary angles and thus it is important to have boundary conditions which have good absorption at all angles of incidents. Also, the point of using a time-domain technique is to obtain wideband information with one run of the algorithm, and therefore it is also important that the ABCs absorb well over the whole range of frequencies which are of interest.

We have implemented both first- and second-order Mur absorbing boundary conditions which were initially developed for the Maxwell equations.[9] Numerical tests with these ABCs in the acoustics case generally reveal a better performance of the second-order conditions over the first. Of course the ABCs are not perfect and small numerical reflections are observed and must be accounted for in numerical results. A brief review of these absorbing boundary conditions as they are applied to the present acoustic wave case follows. The details can be found in Mur's original paper as well as many other expositions.[6,9]

If we consider any scalar field (or component of a vector field), W, which satisfies the second-order wave equation (4), then at the boundary $x=0$ the Mur first-order and second-order boundary conditions are

$$(\partial_x - c^{-1}\,\partial_t)W|_{x=0}=0, \qquad (21)$$

and

$$[c^{-1}\,\partial_{xt}^2 - c^{-2}\,\partial_t^2 - \tfrac{1}{2}\,(\partial_y^2+\partial_z^2)]W|_{x=0}=0, \qquad (22)$$

respectively.

These equations are discretized using second-order centered differences. If we consider one side of our mesh to be terminated by the plane $x=0$, corresponding to the index $i=0$, where only normal components of the velocity vector u_x exist, then the update equations for the first- and second-order Mur ABCs (21) and (22), become

$$u_x^{n+1}(0)=u_x^n(1)+\frac{c\Delta t-\Delta h}{c\Delta t+\Delta h}\,(u_x^{n+1}(1)-u_x^n(0)), \qquad (23)$$

$$u_x^{n+1}(0)=-u_x^{n-1}(1)+\frac{c\Delta t-\Delta h}{c\Delta t+\Delta h}\,(u_x^{n+1}(1)+u_x^{n-1}(0))$$

$$+\frac{2\Delta h}{c\Delta t+\Delta h}\,(u_x^n(0)+u_x^n(1))$$

$$+\frac{(c\Delta t)^2}{2\Delta h(c\Delta t+\Delta h)}\,(\delta_y^2 u_x^n(0)+\delta_y^2 u_x^n(1)$$

$$+\delta_z^2 u_x^n(0)+\delta_z^2 u_x^n(1)), \qquad (24)$$

respectively, where missing spatial indices are half indices, $j+1/2$ and $k+1/2$, in all terms. The finite-difference operators δ_y^2 and δ_z^2 are second-order centered differences used in the approximations of the continuous partial derivatives ∂_y^2 and ∂_z^2 where, for example,

$$\delta_y^2 u_x^n(0)=u_x^n(0,j+3/2,k+1/2)-2u_x^n(0,j+1/2,k+1/2)$$

$$+u_x^n(0,j-1/2,k+1/2), \qquad (25)$$

$$\delta_z^2 u_x^n(1)=u_x^n(1,j+1/2,k+3/2)-2u_x^n(1,j+1/2,k+1/2)$$

$$+u_x^n(1,j+1/2,k-1/2). \qquad (26)$$

Similar expressions can be derived for the absorbing boundary conditions on the remaining five planar sides of the mesh. On the $y=$constant planar boundaries we terminate with u_y velocity components, whereas on the $z=$constant planar boundaries we terminate with u_z velocity components. Note that second-order Mur ABCs cannot be used on the edges of the mesh due to terms such as those given in (25) and (26). Thus, on the edges we always use first-order Mur ABCs.

II. EVALUATION-POINT SOURCE IN AN INFINITE HOMOGENEOUS SPACE

Although the numerical scheme described above can model various source excitations, from a practical point of view, in room acoustics it is typical to model sources of acoustic energy originating from a small sphere or a quasi-point source. In order to evaluate the leapfrog scheme and determine the performance of the absorbing boundary conditions for this type of source, we compare the numerical results of imposing the pressure at a single point in a homogeneous mesh to the analytic solution of a small spherical source radiating in an infinite homogeneous space where the speed of sound is 343 m/s.

The excess pressure everywhere in a homogeneous infinite space produced by a pressure point-source satisfies the inhomogeneous second-order wave equation (4). If we impose the excess pressure as a function of time, say $f(t)$, on a small sphere of radius r_0 centered at the origin, then the pressure outside this sphere is given by

$$p(r,t)=(r_0/r)f[t-(r-r_0)/c], \qquad (27)$$

where r is the radial direction in the mesh.

For our test problem we imposed a time varying pressure at a single point in the grid. We used a grid of size $50\times50\times50$ having $\Delta x=\Delta y=\Delta z=5$ cm, and imposed the pressure at the center of the grid, that is, at ($i=25$, $j=25$, $k=25$). For this and all numerical results described herein, the time step was chosen as the upper bound of the Courant stability limit, (18). Thus, for this grid the time step was set to 84.2 μs. The time variation was chosen to be the derivative of a Gaussian function, given by

$$f(t)=-2\alpha(t-\beta)Ae^{-\alpha(t-\beta)^2}, \qquad (28)$$

and the parameters were set to $\alpha=2.205\,92\times10^6$, and $\beta=2.683\,18\times10^{-3}$. The mesh was truncated using the second-order Mur ABCs and the pressure was sampled at 12 receiver points with coordinates listed in Table I. The geometry of the problem with the 12 receiver locations are shown in Fig. 3. The time-domain waveform of the imposed pressure is shown in Fig. 4 and the calculated waveforms at the points P2, P6, and P10 (see Table I for the coordinate locations and distances from the source), are shown in Fig. 5. Note the relatively small numerical reflections in the time range 0.010–0.015 s originating at the mesh boundaries. These reflections increase in size relative to the size of the primary waveform as we sample at points closer to the mesh boundaries. It is thus important to keep the grid boundaries sufficiently far away from measurement points in order to reduce the effect of these reflections. The performance of the Mur ABCs is better for source waveforms having a lower-frequency content; that is, the magnitude of the reflected wave would be smaller for a source waveform having the same amplitude but slower rise and fall times. Better and more efficient ABCs have been and are continually being developed by researchers solving wave-type problems.[7,9]

As well as giving us insight into the performance of the Mur ABCs for acoustics, our test problem serves to evaluate how well the algorithm models spherical waves produced by a transient point source in the mesh. We see from Table I that a numerical speed equal to the correct speed of 343 m/s is achieved only along diagonal 2 and only for the positive peak of the waveform. It is well known that this direction in the grid gives the best dispersion characteristics when using the leapfrog scheme.[6] The fact that the negative peak seems to travel at a slightly higher speed is probably due to the fact

TABLE I. Peak pressures and velocities for a point source in homogeneous medium.

Point		Grid coordinates (Δh=5 cm)	Distance from source (cm)	Pressure (N/m^2) positive peak negative peak	Time (ms) positive peak negative peak	Avg. Vel. (m/s) positive peak negative peak
	Ref.	(25,25,25)	0	126 939 −126 939	2.188 206 9 3.198 148 5	- -
	P1	(30,25,25)	25	7848.39 −8005.88	2.861 501 3 3.871 442 9	371.31 371.31
Horizontal	P2	(35,25,25)	50	3878.91 −3990.01	3.618 957 5 4.628 899 1	349.47 349.47
	P3	(40,25,25)	75	2561.78 −2683.02	4.376 413 7 5.302 193 5	342.75 356.46
	P4	(46,25,25)	100	1896.72 −2030.26	5.133 869 9 6.059 649 7	339.48 349.47
	P5	(30,30,25)	25√2	5677.21 −5683.99	3.198 148 5 4.123 928 3	350.07 381.90
Diagonal 1	P6	(35,35,25)	50√2	2823.81 −2855.40	4.208 090 1 5.218 031 7	353.55 350.07
	P7	(40,40,25)	75√2	1876.94 −1916.52	5.302 193 5 6.227 973 4	340.61 350.07
	P8	(45,45,25)	100√2	1410.33 −1446.74	6.312 135 2 7.237 915 0	342.93 350.07
	P9	(30,30,30)	25√3	4683.97 −4679.53	3.450 633 9 4.376 413 7	343.00 367.50
Diagonal 2	P10	(35,35,35)	50√3	2345.38 −2343.73	4.713 060 9 5.638 840 7	343.00 354.83
	P11	(40,40,40)	75√3	1563.96 −1562.22	5.975 487 9 6.901 267 8	343.00 350.80
	P12	(45,45,45)	100√3	1176.99 −1158.60	7.237 915 0 8.163 694 8	343.00 348.81

that slower high-frequency waves from the positive peak have merged with the negative peak and as a result have broadened it slightly.

The $1/r$ attenuation of the wave inherent in spherical waves, as shown in Eq. (27), can also be checked for the positive and negative peaks of the waveforms using Table I. A simple check on the accuracy of the algorithm can be made by defining the percent error in the attenuation of the pressure between any two points as

$$\% \text{ Error} = \left(\frac{R_2 P_2}{R_1 P_1} - 1 \right) 100, \tag{29}$$

where R_1 and R_2 are the distances from the source of the first and second point, respectively, and P_1 and P_2 are the calculated pressures at these points. For example, if we assume that the source has zero radius then the percent error between points P9 and P11 can be calculated as 0.169% for the positive peak. We can also define a numerical radius, r_0, of the
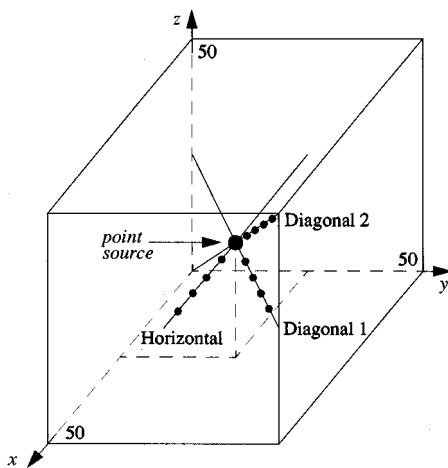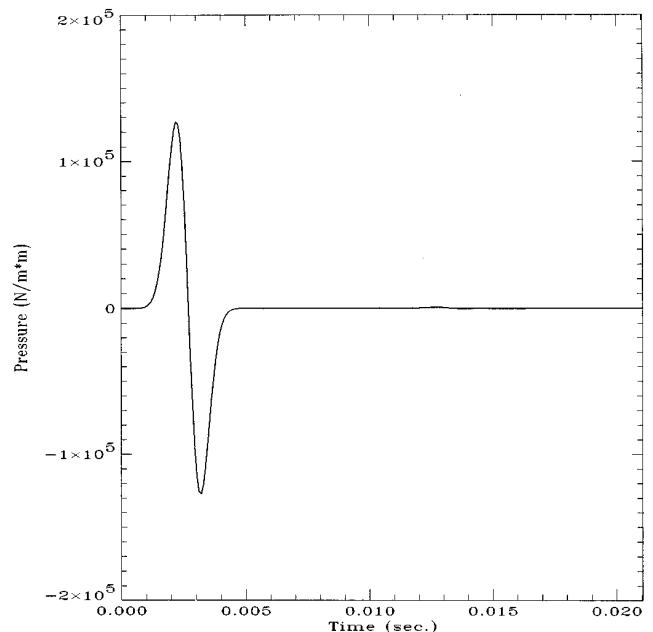

FIG. 3. Validation problem consisting of a point source radiating in a homogeneous medium and the points at which the numerical results were sampled in time.

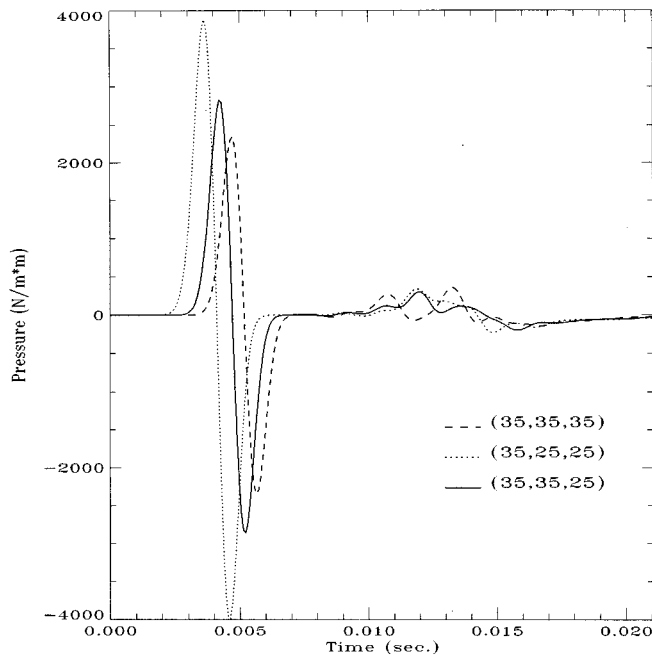FIG. 4. Imposed pressure at the grid point (25,25,25) in a mesh of size 50×50×50.

FIG. 5. Pressures as a function of time at points P2, P6, and P10 on the horizontal and diagonal directions.

point source by imposing that the percent error be zero from r_0 to another point in the mesh. For example, if we assume that the percent error is zero at point P11, then we must have

$$r_0 = \frac{75\sqrt{3}(1563.96)}{12\ 6939} = 1.6 \ \text{cm}. \tag{30}$$

All the points in Table I predict an r_0 of approximately 1.6 cm. Thus, our numerical point source can be thought of as occupying a sphere having a diameter of about 3.2 cm within a 5-cm cubical cell of the mesh.

III. SIMULATION OF THE SEAT DIP EFFECT IN A CONCERT HALL

As an example of a practical room acoustics application of the finite-difference time-domain method; we examine the seat dip effect which is frequently found to occur in concert halls. In 1964, the independent studies of Schultz and Watters[10] and Sessler and West[11] demonstrated that sound waves passing over rows of theatre seats at grazing incidence are subject to selective attenuation of the low frequencies. This dip in the low frequencies can be up to 15 or 20 dB and generally occurs in the frequency range from about 80 to 200 Hz. Both groups concluded that the frequency of the dip is determined primarily by a vertical resonance in the gaps between the rows. A horizontal resonance between the rows was believed to have only a secondary effect. Sessler and West further concluded that a broadband absorption at frequencies from 80 to 400 Hz results from diffraction of the sound waves around the upper edges of the seats. More recently, Ishida[12] conducted a time-domain experimental investigation of the seat dip effect using a simplified physical model. He concluded that the seat dip attenuation was caused by interference between the direct sound wave and a nega-

tive pressure wave. The negative pressure wave was shown to be due to the diffraction around the tops of the seat backs.

As such, the underlining mechanisms which create the seat dip effect make it unsuitable for analysis by ray tracing or image source methods. Conversely, the seat dip effect lends itself ideally to analysis by the finite-difference time-domain method since it is a low-frequency wave phenomenon, and it primarily affects the direct sound; so the response of the entire concert hall does not need to be modeled. Therefore, as further validation of our model, we report the results of simulations conducted to demonstrate how the finite-difference time-domain method can accurately predict the various aspects of the seat dip effect.

There have been several previous studies wherein the seat dip effect has been modeled using theoretical (rather than scale model measurements) approaches. Ando et al.[13] simulated a plane wave passing over a periodic boundary of infinite length. The authors of that study concluded that the severity of the seat dip effect could be reduced by using absorbing floor surfaces. More recently, Terai and Kawai[14] used boundary element methods to model various seating configurations in both two and three dimensions and compared their results to measurements made using scale models. However, the results predicted by their theoretical model diverge significantly from the results of their scale model measurements.

In the present study, two simulations were conducted. In the first simulation, an omnidirectional point source, S, was located in the center of the stage at a height of 100 cm above the floor. In the second simulation the source was set to a height of 250 cm above the floor. All other parameters were held constant between the two simulations. A total of 18 receiver locations were distributed throughout the 16 rows of seats, as shown in Fig. 6. Receiver heights of 110, 200, and 300 cm were used. A detailed view of how the rows were placed in the finite-difference grid is shown in Fig. 7. The scattered field formulation was used and an incident pressure field originating at the source point, S, was assumed with a time-domain variation given by the derivative of a Gaussian function.

The cubical grid size used in the simulations was 5 cm, giving an upper frequency limit of about 1400 Hz. The grid dimensions were $490 \times 70 \times 85$ for a total grid size of 2 915 500 cells. A time step of $8.41\ 618 \times 10^{-5}$ s was used in the simulations which were run for 1500 time steps. Therefore, the first 126 ms or so of the impulse responses were calculated. The results of the simulations are shown in Figs. 8, 9, and 10. A very modest smoothing (approximately 1/10th octave) was applied to the curves in these figures and their levels have been normalized. This was done solely to improve visual clarity and to make it easier to identify the center frequency of the dips.

Figure 8 illustrates the effects of the distance from the source to the receiver on the seat dip effect. The figure shows the transfer functions from the source to six receiver points located at different locations among the rows of seats. The distance from the source to the first receiver was 7 m while the distance to the last receiver was 18.9 m. The transfer functions were obtained by taking the Fourier transforms of
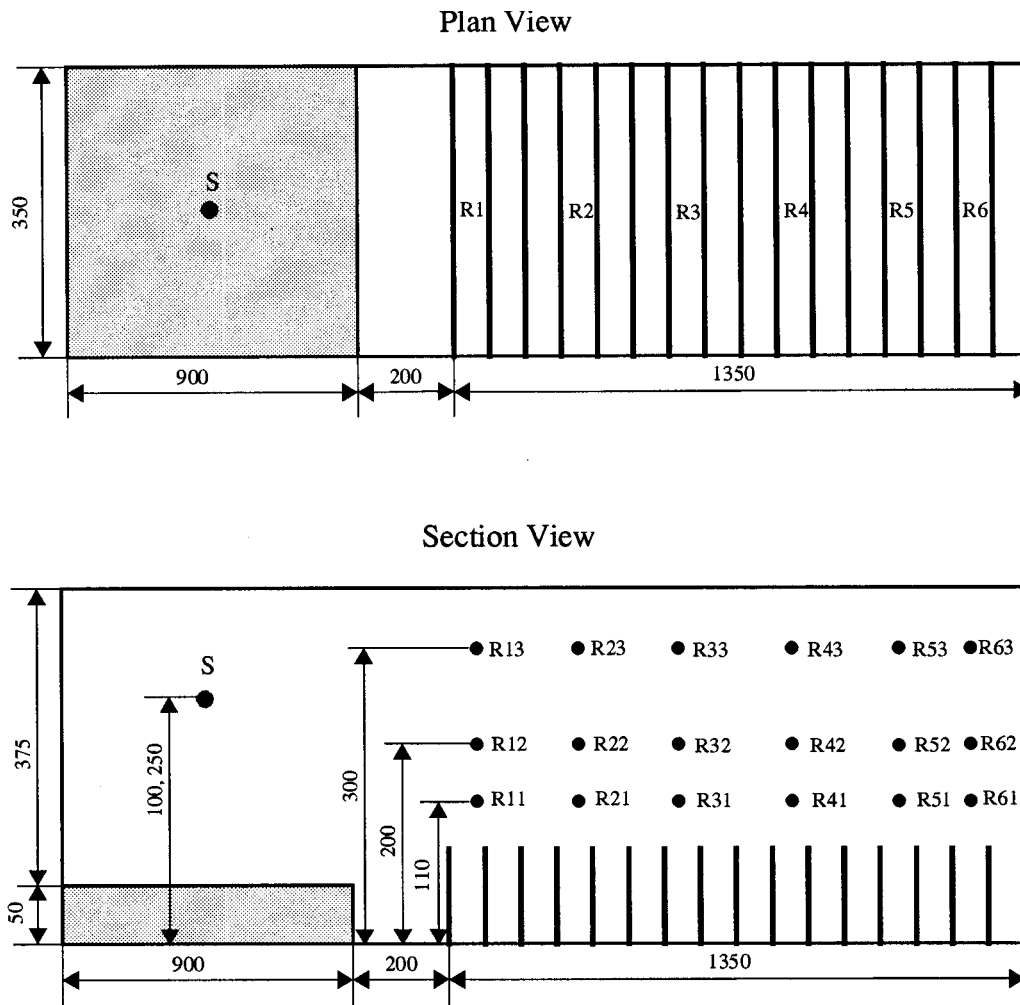
Plan View

Section View

FIG. 6. Plan and section views of the 16 row plus stage model used in the simulations showing the source, S and the 18 receiver positions, Rxx. Two source heights (100 cm and 250 cm) were modeled. Receivers were placed at 110 cm, 200 cm, and 300 cm.

the impulse responses derived from one of the simulations (source height=250 cm). The figure clearly shows a dip in each of the transfer functions in the frequency range between about 80 and 200 Hz as anticipated.

The figure also shows that the low-frequency dip be-

comes more pronounced (deeper) as the sound wave travels over more and more rows of seats. This result is in exact agreement with the findings of both Schultz and Watters, and Sessler and West. It can be further seen from Fig. 8 that the
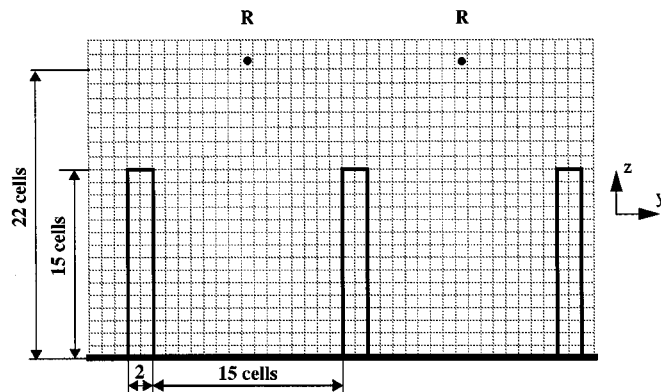

FIG. 7. Rows of chairs modeled in the finite-difference grid. Distance between rows is 75 cm. The seat thickness is 10 cm and the row height is 75 cm. The receivers which are shown are at a height of 110 cm. Cubical cells 5 cm in size were used.
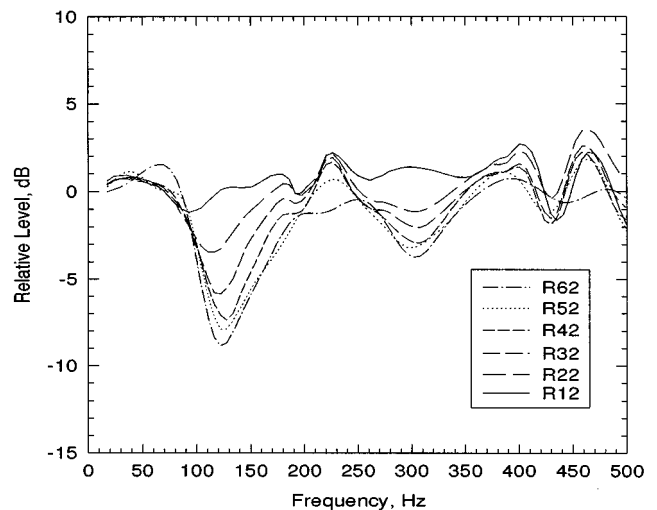

FIG. 8. Transfer functions from the source to six receiver positions, illustrating the effect of distance (or grazing angle) on the seat dip. R12 is nearest to the source while R62 is furthest from the source.
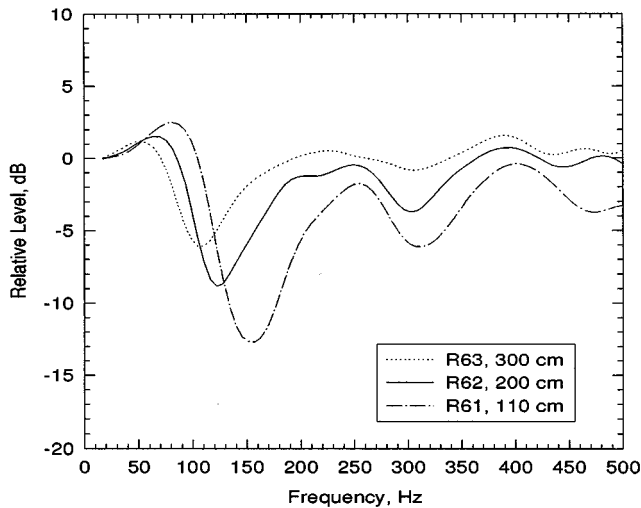
FIG. 9. Transfer functions from the source to three receiver positions, illustrating the effect of the height of the receiver on the seat dip.

frequency of the dip increases as the distance between the source and the receiver increases. Another way of viewing this is to note that the frequency of the dip increases as the grazing angle is decreased. Also, the curves of the figure show that the dip becomes narrower as the grazing angle is increased. These related results were found by Schultz and Watters and by Bradley[15] for both scale model measurements and measurements in real concert halls. Therefore, the computer model using the finite-difference time-domain method is able to successfully model the seat dip phenomenon and these three effects due to the source–receiver distance. Interestingly, the theoretical analysis by Ando et al. failed to predict any dependence of the dip frequency on the grazing angle even though they simulated a 20° range of grazing angles (see Fig. 5, Ref. 13).

In both of the 1964 studies the effect of the receiver height was examined and it was found that the depth of the

low-frequency dip decreases as the height of the receiver is increased. Schultz and Watters conducted a more detailed analysis and their results further show that the frequency of the dip decreases as the height of the receiver is increased above the rows of seats. Therefore, the effect of the receiver height was also examined in the present study. Figure 9 shows the transfer functions from the source to the three receiver points, R61, R62, and R63 derived from our computer simulations. All three receivers are located in the last row of seats with R61 at a height of 110 cm, R62 at a height of 200 cm, and R63 at a height of 300 cm. The simulation with the source set to a height of 250 cm was used for this analysis. The curves of Fig. 9 clearly show the depth of the low-frequency dip decreasing as the receiver height is varied from 110 cm to 300 cm. Also seen in the figure is the downward shift in the frequency of the dip as the height of the receiver is increased. These results demonstrate that our computer model is able to correctly predict these two effects due to receiver height.

As a final verification of our model's ability to accurately simulate the various components of the seat dip effect, we examined the effect of the height of the source. It should be noted that a change in the source height can be viewed equivalently as a change in the grazing angle of the sound. Both Schultz and Watters and Bradley conducted tests to specifically examine this parameter. In those studies it was found that an increase in the height of the source resulted in a decrease in the frequency of the dip. Figure 10 shows the results of the present study examining the effect of the height of the source. The solid curve of the figure shows the transfer function to the receiver point, R61, with the source set to a height of 250 cm, while the dashed curve is the transfer function to the same receiver but with the source set to 100 cm. As can be seen from the figure, increasing the height of the source has resulted in a lowering of the frequency of the dip. Specifically, the frequency of the dip has gone from about 175 Hz down to about 150 Hz. Therefore, the effect of the source height has been correctly predicted by the computer model.

In his 1991 study, Bradley,[15] made measurements in a concert hall to find the relation between the seat dip effect and the height of the source. He did this for several receiver positions in the hall. Bradley found that the results for all the receiver positions could be collapsed into a single trend by plotting the frequency of the main dip versus the grazing angle of the direct sound (see Fig. 2, Ref. 15). The results from our simulations (receiver height 110 cm) were therefore plotted in terms of the frequency of the main dip versus the grazing angle of the direct sound to see if this trend could be replicated. Figure 11 shows that the results of the present simulations do indeed display a trend which is very similar to that found experimentally by Bradley.

The results of the computer simulations demonstrate that the finite-difference time-domain method was able to successfully and accurately predict various aspects of the seat dip effect. None of these effects can be modeled using either ray tracing or the image source method. While the intent of this section was not to contribute new work to the under-
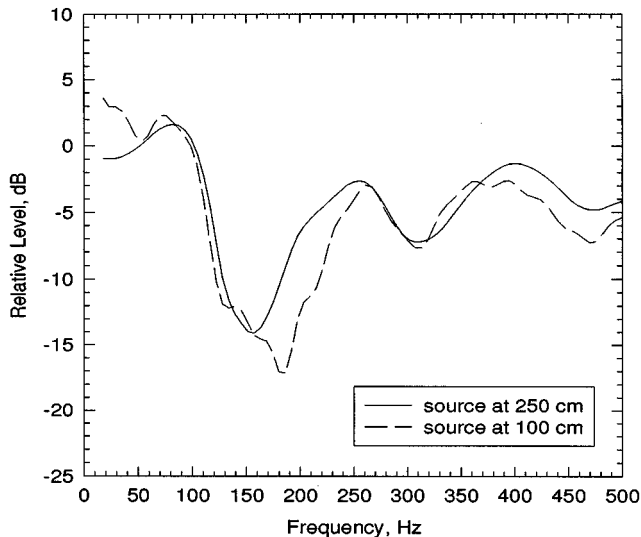

FIG. 10. Transfer functions from two different source locations to receiver R61, illustrating the effect of the height of the source on the seat dip.
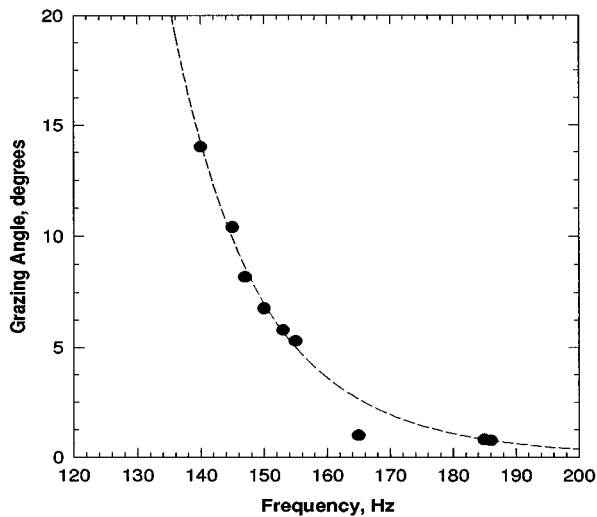
FIG. 11. Grazing angle versus dip frequency calculated using the finite-difference time-domain method. Receiver points at a height of 110 cm.

standing of the seat dip effect, it is clear that the finite-difference time-domain method could serve as a valuable tool in such an effort. The method is useful in the analysis of any low-frequency phenomenon where the true wave nature of the propagation of sound in a room is required.

IV. CONCLUSIONS

In this paper a finite-difference time-domain solution of the acoustic wave equations was derived including expressions for material boundary conditions and absorbing boundary conditions. Second-order Mur absorbing boundary conditions were used and the resulting limitations were described and demonstrated. The implications of these imperfect absorbing boundary conditions were discussed. The model was validated using the analytical solution of a free space pressure point source.

Computer simulations of the well-known seat dip effect in concert halls were conducted using the finite-difference time-domain method. The results of the computer simulations were compared with the findings of previous studies where measurements had been made on scale models and in real concert halls. It was shown that the computer model successfully predicts the effects of the source–receiver distance, the height of the receiver, and the height of the source. The results of the simulations provide further confirmation of

the validity of the model and demonstrate the usefulness of the method in the analysis of a practical room acoustics problem. The finite-difference time-domain method is a useful tool in the analysis of low-frequency room acoustic phenomenon where the true wave nature of sound must be accurately modeled.

ACKNOWLEDGMENTS

[1] H. Kuttuff, ''Sound field prediction in rooms,'' in *15th International Congress on Acoustics*, Trondheim, Norway, Vol. II, pp. 545–552 (1995).
[2] G. Naylor (Guest editor), Special Issue on ''Computer modeling and auralization of sound fields in rooms,'' Appl. Acoust. **38**, 2–4 (1993).
[3] J. J. Bowman, T. B. A. Senior, and P. L. E. Uslenghi, *Electromagnetic and Acoustic Scattering by Simple Shapes* (revised printing) (Hemisphere, New York, 1987).
[4] L. B. Felsen and N. Marcuvitz, *Radiation and Scattering of Waves* (Prentice-Hall, Englewood Cliffs, NJ, 1973).
[5] K. S. Yee, ''Numerical solution of initial boundary value problems involving Maxwell's equations in isotropic media,'' IEEE Trans. Ant. Propagat. **AP-14** (4), 302–307 (1966).
[6] K. S. Kunz and R. J. Luebbers, *The Finite Difference Time Domain Method for Electromagnetics* (CRC, Boca Raton, FL, 1993).
[7] J. G. Maloney, and K. E. Cummings, ''Adaptation of FDTD Techniques to Acoustic Modeling,'' in *11th Annual Review of Progress in Applied Computational Electromagnetics*, Vol. 2, Monterey, CA, 724–731, March (1995).
[8] G. Mur, ''Absorbing boundary conditions for the finite-difference approximation of the time-domain electromagnetic-field equations,'' IEEE Trans. Electromagn. Compat. **EMC-24** (4), 377–382 (1981).
[9] R. L. Higdon, ''Numerical absorbing boundary conditions for the wave equation,'' Math. Comput. **49**, 65–90 (1987).
[10] T. J. Schultz and B. G. Watters, ''Propagation of sound across audience seating,'' J. Acoust. Soc. Am. **36**, 885–896 (1964).
[11] G. M. Sessler, and J. E. West, ''Sound transmission over theater seats,'' J. Acoust. Soc. Am. **36**, 1725–1732 (1964).
[12] K. Ishida, ''Investigation of the fundamental mechanism of the seat-dip effect using measurements on a parallel barrier scale-model,'' J. Acoust. Soc. Jpn. (E) **16**(2), 105–114 (1995).
[13] Y. Ando, M. Takaishi, and K. Tada, ''Calculations of the sound transmission over theater seats and methods for its improvement in the low-frequency range,'' J. Acoust. Soc. Am. **72**, 443–448 (1982).
[14] T. Terai and Y. Kawai, ''BEM Applications in Architectural Acoustics,'' in *Boundary Element Methods in Acoustics*, edited by R. D. Ciskowski and C. A. Brebbia (Elsevier, New York, 1991).
[15] J. S. Bradley, ''Some further investigations of the seat dip effect,'' J. Acoust. Soc. Am. **90**, 324–333 (1991).